IEEE Access
Multidisciplinary ⋮ Rapid Review ⋮ Open Access Journal

Received March 17, 2019, accepted April 3, 2019, date of publication April 15, 2019, date of current version April 25, 2019.

Digital Object Identifier 10.1109/ACCESS.2019.2910538

Quantitative Detection of Rock Crack Width Using Microwave Resonance Vibration Eigenvalues

CHUANJING OU[1], PING CAO[1], YU CHEN[1], JINFENG HE[2], XIANWEN LIAO[3], HONGCAI CHEN[2], AND JINGJING MENG[1]

[1]School of Resources and Safety Engineering, Central South University, Changsha 410083, China
[2]Guangxi Electronic Products Quality Inspection Center, Beihai 536000, China
[3]School of Information and Communication, Guilin University of Electronic Technology, Guilin 541004, China

Corresponding authors: Ping Cao (pcao_csu@sina.com) and Yu Chen (yu.chen@csu.edu.cn)

This work was supported in part by the National Natural Science Foundation of China under Grant 11772358 and Grant 51604299, in part by the China Postdoctoral Science Foundation under Grant 2018T110846, and in part by the Independent Innovation Project of Graduate Students in Central South University under Grant 2016zzts101.

ABSTRACT To accurately detect micro crack widths in rocks in real time, a new method based on a microwave resonance vibration model is proposed. Repeated experiments carried out by the developed microwave resonance vibration model-based sensor and the measuring apparatus determined that the center frequency of this model is 3.665 GHz. The experimental verification on various crack widths (below 1 mm) is performed after the calibration experiment of taking the plug gauge and dial gauge as standard. The relationship between the actual value and the amplitude of the output voltage of the microwave signal is analyzed; in addition, the influence of different environmental relative humidity and specimen water content on rock crack width measurement results is discussed. The experimental results show that, under the condition of a resonance vibration frequency of 3.575 GHz, the proposed method can accurately and directly determine the micro crack width in rocks. The detection system is developed with a relative error of less than $\pm 5\%$, the minimum value of stability detection is 50 μm, and the fastest response speed of 0.28 ns. In terms of the influence of different environmental relative humidity and specimen water content on the measurement results, the greater the relative humidity, the higher the specimen water content, and the greater the influence on the measurement results. It provides an important reference for rock crack width variation monitoring and serves well for the rock masses engineering stability evaluation.

INDEX TERMS Microwave resonance vibration model, output voltage, rock crack width, sensor.

I. INTRODUCTION

Rock masses contain numerous microscopic and macroscopic discontinuities, such as cracks, joints and faults. Many field engineering projects have shown that unstable failure can easily start from these pre-existing discontinuities. For example, changes in the stress in rock masses caused by disturbances from site excavation may result in new cracks, or the original cracks may extend, propagate, and even cause unstable damage. Hence, the failure of the rock masses is heavily affected by the pre-existing discontinuities. Deformation monitoring of rock masses plays a key role in the study of pre-existing discontinuities and can help people understand the fracture mechanism and assess the stability of fractured rock masses.

The determination of crack width in rock precisely is one of the effective approaches for deformation monitoring of rock masses. In order to understand the fracture mechanism, it is especially important to gain insight into the behavior of rock micro crack width changes. The indoor monitoring methods for rock crack width mainly include high-speed photography [1], [2], computed tomography (CT) scanning [3], [4], acoustic emission (AE) detection [5]–[8], nuclear magnetic resonance (NMR) [9]–[11], and scanning electron microscope (SEM) [12], [13]. The most obvious advantage of high-speed photography is their direct observation characteristics, but the crack width values cannot be directly quantified, while this value is quantified by software post-processing. Compared with the use of CT scanning, NMR, and SEM, AE detection records the triggering events in real time. The AE detection system starts to record after the trigger event accumulating a certain amount, which means there will be a certain delay. It is

The associate editor coordinating the review of this manuscript and approving it for publication was Jiafu Wan.

not difficult to find that the use of AE detection to quantify micro crack still has drawbacks. The costs of using the above techniques are still high. It would be of considerable benefit if developments of new crack width monitoring technique could quantify the cracks in real-time simply and economically. In summary, deep insight into the study of rock micro crack width change is still not comprehensive enough.

Microwave techniques have been applied to monitor crack size, where the determination of metal defects is the most common [14]–17]. In addition, the microwave non-destructive testing (NDT) method also has certain applications in the field of civil engineering [18]–[32]. These studies mainly explore the generation of electromagnetic radiation accompanying the fracture process of the specimen under the action of external loading and determine the crack development by detecting the energy intensity of the electromagnetic wave. However, active electromagnetic waves are rarely used. WANG *et al*. [33] and LV *et al*. [34] use the electromagnetic wave for acting on the specimen and then detect the energy intensity of the electromagnetic wave absorbed by the specimen to judge the crack condition. For the study of quantifying micro crack widths, microwave scattering method only has a small part of the incident electromagnetic field interacting with the crack, and the interaction is very weak, so it is easily affected by external interference, resulting in inaccurate detection results. Therefore, monitoring technique must be able to fully capture and record events in a short period of time. After analyzing the existing microwave-based techniques, it should be noted that accurate detection and characterization of micro crack still pose a challenge in rock crack width variation monitoring.

In view of this, a new microwave resonance vibration model-based detection for rock crack width was proposed. Then, the experimental verification of different rock crack widths from 0 to 1mm is carried out to realize the real-time quantification of rock micro crack width. This new approach can provide more accurate information in a shorter time. It offers a new reference of developing a highly accurate and intelligent determination method in the field of civil engineering.

II. DESCRIPTION

A. PPRINCIPLE OF MEASURING ROCK CRACK WIDTH BASED ON MICROWAVE RESONANCE VIBRATION MODEL

The rock specimens are mounted in parallel with the microwave resonance vibration model-based sensor of rock crack width monitoring, which is a non-contact technique, and the standoff distance (D) between the two is 0.1 mm, as seen in Fig. 1. Fig. 1 is the installation relationship in a microwave resonance vibration model-based measuring apparatus. On the basis of considering the essential properties of the tested specimen, the standoff distance (D) of 0.1 mm is determined by repeated experiments, so that the magnetic lines of force are incident on the rock as perpendicular as possible, thereby ensuring the sensor sensitivity [29].

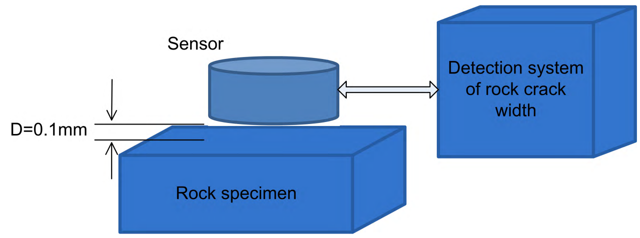

FIGURE 1. Installation relationship in a microwave resonance vibration model-based measuring apparatus.

The essence of microwave resonance vibration model-based measurement of rock crack width is to use electromagnetic waves from the sensor to couple with rock specimens. The reason is to make the magnetic dipole and electronic dipole in the rock specimen resonate with it. That is, a coupled microwave magnetic field is generated in a rock specimen. When a crack occurs in the rock specimen, it can be visualized as a rectangular waveguide, and the rock crack width determined by the microwave resonance vibration model is theoretically analyzed with reference to the waveguide analysis method [15], [16]. Given that the sensor sensitivity range of the microwave resonance vibration model is relatively small, it is particularly suitable for measuring the micro crack width. If you want to measure a wide range of rock crack widths from micro-small to large, it is necessary to take the combination of electromagnetic wave scattering method and microwave resonance vibration model [33], [34], which can suitably determine the rock crack width of various sizes.

To facilitate a clear understanding of the principles of this new method, the Maxwell equation is first used to theoretically analyze the method of detecting rock crack width by electromagnetic wave scattering to understand the measurement of micro crack width based on microwave resonance vibration model [35]. It is assumed that the microwave propagating to the surface of the rock specimen is a plane wave $\boldsymbol{E}$, and its expression is

$$E = E_0 \, e^{-j\omega t - \gamma x} \tag{1}$$

where $\boldsymbol{E}$ is the electric field strength vector, E_0 is the electric field strength amplitude value, which is a constant, γ is the propagation constant in space, x is the propagation distance along the x-axis, $j\omega$ is the resonance vibration angular frequency, and t is the time required for one oscillation cycle.

The electric field intensity vector $\boldsymbol{E}$ periodically changes with $f = \omega/(2\pi)$ in the time domain, and spatially propagates in the x-axis direction with the propagation constant γ. Then, the propagation constant γ can be expressed as

$$\gamma = \alpha + j\beta = j\omega\sqrt{\mu\varepsilon(1 + \frac{\sigma}{j\omega\varepsilon})} \tag{2}$$

where γ is the propagation constant in space, α is the decay constant, $j\beta$ is the phase constant, σ is the conductivity, $j\omega$ is the resonance vibration angular frequency, ε is the dielectric constant, and μ is the magnetic permeability.

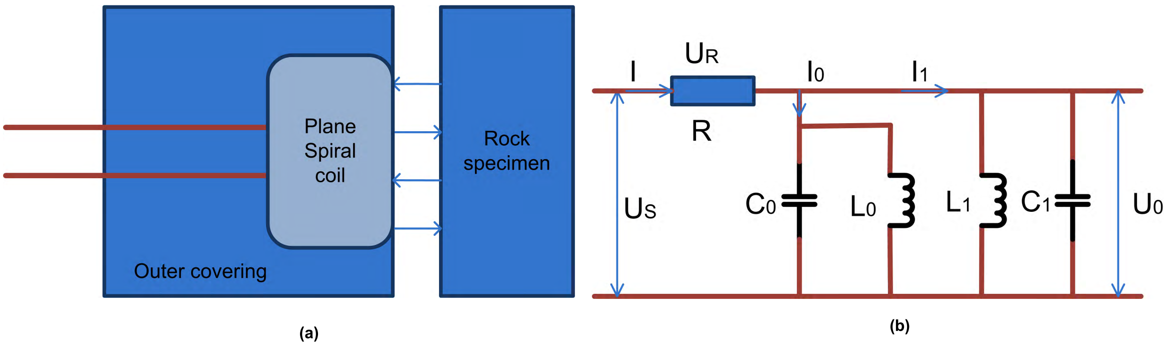

FIGURE 2. Coupling relationship between rock specimen and microwave resonance vibration model-based sensor: (a) schematic diagram of the principle for microwave resonance vibration model-based sensor coupling with rock specimen and (b) equivalent circuit schematic of sensor coupling with rock specimen. U_S is the equivalent output voltage of the microwave resonance oscillation signal, R is equivalent total resistance, L_0 is the sum of the equivalent of sensor inductance and distribution parameter, and C_0 is the sum of the equivalent of the distribution parameters of sensor and resonance oscillation circuit capacitance, L_1 is distributed inductance after the test specimen is loaded, analogously,
C_1 is distributed capacitance after the test specimen is loaded, and U_0 is resonance vibration output voltage. And I is total current, I_1 is load current, I_0 is no-load current, U_R is equivalent total resistance voltage.

When $\sigma/(j\omega\varepsilon) \gg 1$, "(2)" can be written as

$$\gamma = \sqrt{j\omega\mu\sigma} \quad (3)$$

The ratio of the electric field strength vector $\boldsymbol{E}$ to the magnetic field strength vector $\boldsymbol{H}$ is equal to the wave impedance $\boldsymbol{Z}$, and when $\sigma = j\omega\varepsilon$, that is

$$Z = \frac{E}{H} = \frac{\gamma}{j\omega\varepsilon} = \sqrt{j\omega\mu/\sigma} \quad (4)$$

where $\boldsymbol{Z}$ is the wave impedance, $\boldsymbol{E}$ is the electric field strength vector, and $\boldsymbol{H}$ is the magnetic field strength vector.

In the rock specimen, when the amplitude of the field strength is rapidly reduced to the original value by $1/e$ times, the corresponding depth d is called the microwave penetration depth, that is

$$d = \sqrt{2/(\mu\omega\sigma)} \quad (5)$$

In addition to penetration, the reflected wave coefficients need to be considered. The reflection coefficient Γ can be expressed by that of the light wave

$$\Gamma = \frac{Z_2 - Z_1}{Z_2 + Z_1} \quad (6)$$

where Γ is the reflection coefficient, Z_1 is the air dielectric wave impedance, Z_1 is expressed as $Z_1 = \sqrt{\mu_0/\varepsilon_0}$, and Z_2 is the wave impedance in rock specimen, expressed as $Z_2 = \sqrt{\mu/\varepsilon}$.

As the rock specimen is not an ideal reflector (for example, metal is one of the ideal reflectors), the reflection coefficient is very small when the electromagnetic wave is perpendicularly incident on the rock specimen, namely, its reflection coefficient $\Gamma \neq -1$ (negative sign indicates the opposite direction to the incident direction). If there is a crack on the surface of rock specimen, a part of the electromagnetic wave is scattered, and the amplitude of the scattered wave signal is also small; it is not suitable for reliable detection of the micro crack. However, this method is applicable when the crack width increases to a certain extent.

To effectively measure the micro small rock crack width, the microwave resonance vibration model-based method for determining rock crack width is proposed. The following is the theoretical analysis of this new method. Fig. 2 shows the coupling relationship between a rock specimen and a microwave resonance vibration model-based sensor. To facilitate theoretical analysis, the schematic diagram of the principle for microwave resonance vibration model-based sensor coupling with the rock specimen in Fig. 2(a) is abstracted into the equivalent circuit in Fig. 2(b). Us is the equivalent output voltage of the microwave resonance oscillation signal, R is the equivalent total resistance, L_0 is the sum of the equivalent of sensor inductance and distribution parameter (which is a key component in generating microwave magnetic fields), C_0 is the sum of the equivalent of the distribution parameters of sensor and resonance oscillation circuit capacitance, L_1 is the distributed inductance after the test specimen is loaded, analogously, C_1 is the distributed capacitance after the test specimen is loaded, and U_0 is the resonance vibration output voltage. The microwave resonance vibration model for determining rock crack width changes the resonance oscillation frequency f_0 by changing the distributed inductance L_1 and distributed capacitance C_1 of the resonance oscillation network, thereby realizing the crack width detection. However, in general, measuring the distributed inductance and distributed capacitance are not as convenient as measuring the resonance oscillation voltage or phase angle. Therefore, when working, the microwave resonance vibration model-based sensor is in a state of no-load set resonance oscillation if it is not loaded with a specimen, and its resonance oscillation angular frequency is represented by ω_0, which is characterized as

$$\omega_0 = \sqrt{1/(L_0 C_0)} \quad (7)$$

where ω_0 is the resonance oscillation angular frequency, L_0 is the sum of the equivalent of sensor inductance and distribution parameter, and C_0 is the sum of the equivalent of the

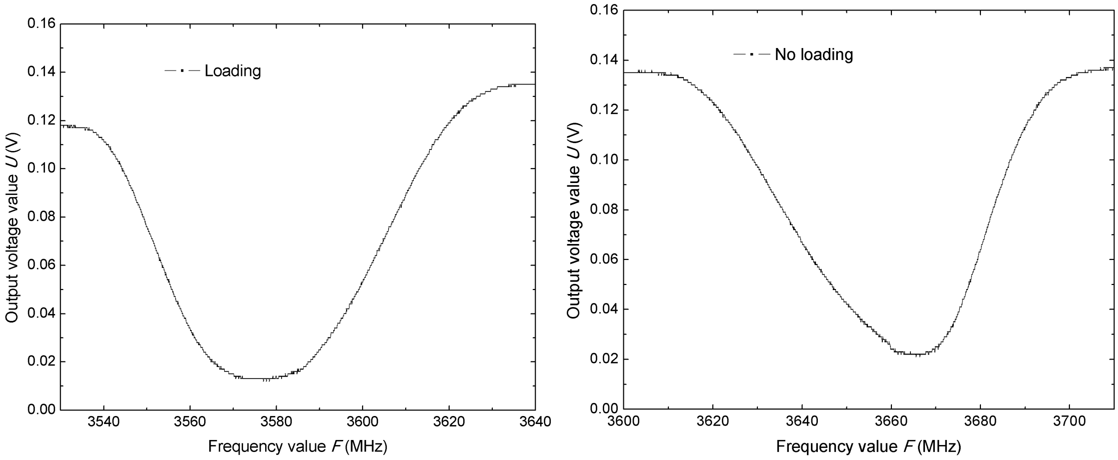

FIGURE 3. Relationship curve between output voltage value *U* (V) and frequency value *F* (MHz) of measuring apparatus: (a) loading granite rock specimen with crack-free and (b) at no load.

distribution parameters of sensor and resonance oscillation circuit capacitance.

The resonance oscillation frequency is expressed as f_0, and its expression is

$$f_0 = \frac{1}{2\pi}\sqrt{1/(L_0C_0)} \quad (8)$$

As we see in Fig. 1, after loading the test specimen, the electrons in the rock specimen are subjected to electromagnetic energy and are arranged to move and absorb energy. At this time, the load current I_1 of the equivalent circuit in Fig. 2(b) increases and total current I increases accordingly, U_R increases, but U_0 decreases. The absorbed energy of the electrons in the rock specimen under different frequencies is different, the total current I is also different, and U_0 changes with I as well. Therefore, the frequency of the microwave signal source changes to reduce the energy absorption to the lowest point (the bottom of the valley). Accordingly, as the frequency continues to increase, the absorbed energy of the electrons in the rock specimen increases from the bottom. The valley point in this process is called the resonance vibration point, see Fig. 3. The results of granite crack width measurement data are displayed in Fig. 3 to illustrate the above situation. Fig. 3(a) is a graph showing the relationship between output voltage value U(V) and frequency value F(MHz) of the measuring apparatus at the condition of loading rock specimen with crack-free. Fig. 3(b) is the one under the condition of no load. It should be pointed out that in order to capture micron-scale crack width information easily, the resonance oscillation point characteristics of the sensor are preferably designed. In that case, the resonance point is not a single-valued cusp, while it has a relatively smooth small range. The amplitude of the output voltage signal by the sensor at the time of resonance vibration is recorded as U_0. Its expression is

$$U_0 = U_S - U_R \quad (9)$$

$$U_0 = E = E_0\, e^{-j\omega t - \gamma x} \quad (10)$$

where U_0 is the resonance vibration output voltage, U_S is the equivalent output voltage of microwave resonance oscillation signal, and U_R is the equivalent total resistance voltage.

It can be observed from Fig. 3 that the resonance oscillation frequency f_0 at no load is 3.665 GHz and the offset of f_0 becomes 3.575 GHz after loading, that is, the phase is shifted. In addition, the voltage amplitude U_0 changes accordingly. When no load occurs, the voltage amplitude U_0 is slightly lower than 0.02 V; after loading a specimen, the voltage amplitude U_0 is lower more than 0.02 V. As the rock crack width increases, the voltage amplitude U_0 decreases. This provides us with the possibility to quantify the change of rock crack width.

In short, the variation of rock crack width is evaluated based on the magnitude of U_0, which is extremely convenient. In summary, during the process from rock crack initiation to propagating until eventual failure, the initial stage of crack initiation could be suitably measured by microwave resonance vibration model. After that initial period, the combination of microwave resonance vibration model-based method and microwave scattering method can obtain satisfactory results.

B. MATERIALS

Granite is used as the test material. Granite is mainly composed of quartz, K-feldspar, plagioclase and biotite, and it is meat red. It has a medium-fine grain granitic structure and a block structure, as shown in Fig. 4.

There are two types of experimental specimens in the rock crack width detection test. One is defined as a regular crack, which is a straight crack with a flat fracture surface, and the other is defined as an irregular crack, which is extended or propagated in an asymmetric state. The regular crack test specimen was prepared by directly cutting the square granite (Length × width × height = 150 mm × 45 mm × 20 mm) into two halves with a diamond saw blade.

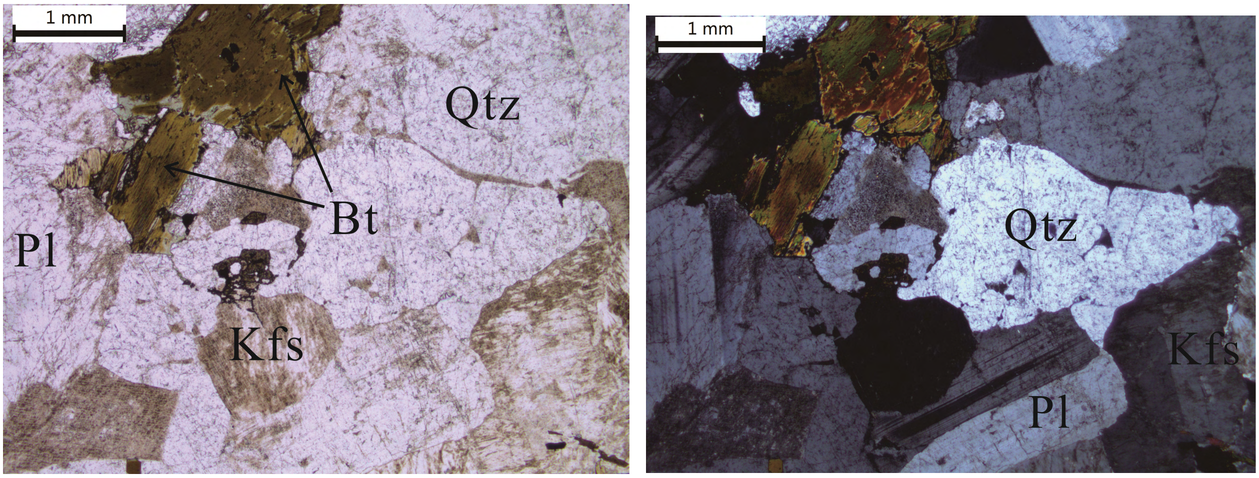

(a) (b)

FIGURE 4. **Photomicrograph of granite: (a) single polarized photomicrograph and (b) orthogonally polarized photomicrograph.**

FIGURE 5. **Processing of irregular crack specimen.**

The irregular crack test specimen was fabricated as follows. First, the semi-disc test specimen having a radius of 49 mm and a thickness of 21 mm was machined, and a straight crack was prefabricated in the middle, as shown the specimens in Fig. 5. Afterwards, an irregular crack test specimen was prepared by a three-point bending test on the semi-disc test specimen by a microcomputer-controlled pressure testing machine WHY-200/10, see Fig. 5. The non-parallelism of the top and bottom planes of the test specimen was prepared within $\pm 2\ \mu$m. In addition, the geometrical dimensions of the rock specimen tested can satisfactorily cover the detection range of the microwave resonance vibration model-based sensor.

C. MEASURING APPARATUS AND EXPERIMENT PROCEDURE SETUP

The experiment was carried out on a precision mobile test platform (length $\times$ width $=$ 290 mm $\times$ 76 mm) and a mechanical runout of $\pm$ 2 μm. The precision mobile test platform includes two parts: the mobile support platform and the stationary support platform. The test specimen is fixed on the mobile platform with a jig, as shown in Fig. 6. Then set the

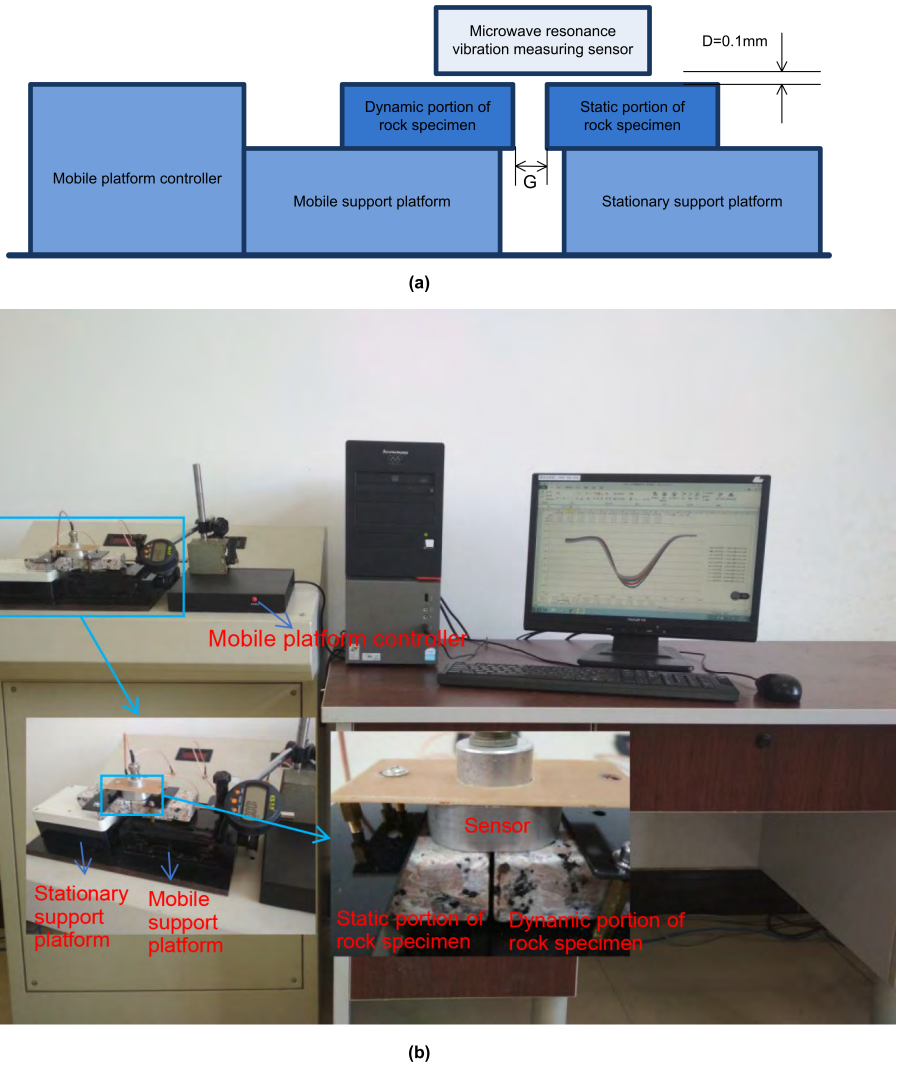

FIGURE 6. **Microwave resonance vibration model-based measuring apparatus: (a) schematic diagram of a simulated mobile platform for rock crack widths measuring apparatus and (b) physical picture of measuring apparatus.**

measured value G, start the experiment and record the data. The details are described below. Fig. 6 includes a schematic diagram of a simulated mobile platform for rock crack width measuring apparatus in Fig. 6(a) and a physical picture of the measuring apparatus in Fig. 6(b). It can be seen from Fig. 6(a) that the distance between the dynamic portion and the static portion of rock specimen is denoted as G, and the distance can be adjusted by manually or automatically moving the platform, and the maximum adjustable distance range is 0-25 mm. The present study mainly focuses on evaluating the accuracy of micro crack width measurement in rocks, along with aiming at providing the new access of capturing cracks initiation in the specimen. Thus, the maximum adjustable distance of the test platform is set to 25 mm. The test platform is used to provide conditions that simulate different crack widths of rock specimen. The sensor for measuring rock crack widths is mounted above the static portion of the test specimen, and the sensor does not come into contact with the crack of the test specimen. In addition, the standoff distance D is 0.1 mm.

The present study designs a crack width determination test for two forms of cracks, including regular and irregular crack fracture patterns. First, the experiment focuses on the determination of the rock crack width in granite with the regular fracture, and its results are presented in section III. Second, the rock crack width measurement of irregular crack specimens is also discussed.

In the experiment of regular straight cracks, first, the plug gauge and the dial gauge were used as the standard and the experimental calibration was performed. The resolution power of the dial gauge is 1 μm. The experimental ambient temperature was 29 °C and the environmental relative humidity was 44.8 %. The first is carried out by using the standard of plug gauge. Rock crack widths of 0 to 1 mm

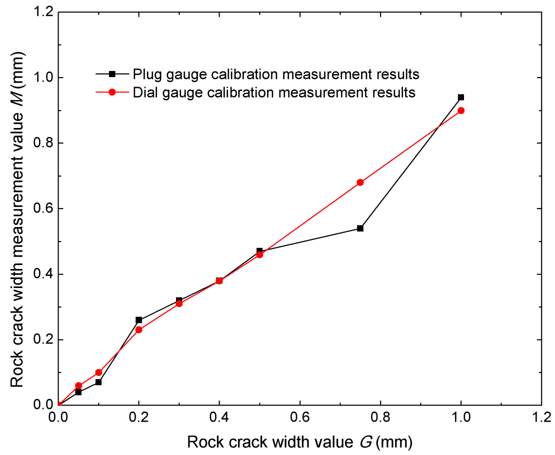

FIGURE 7. Comparison of the two experimental calibration methods. It shows the relationship curve between the rock crack width actual measurement value *M* (mm) of measuring apparatus and the crack width value *G* (mm) of granite, and the calibration is made by taking plug gauge or dial gauge as a standard.

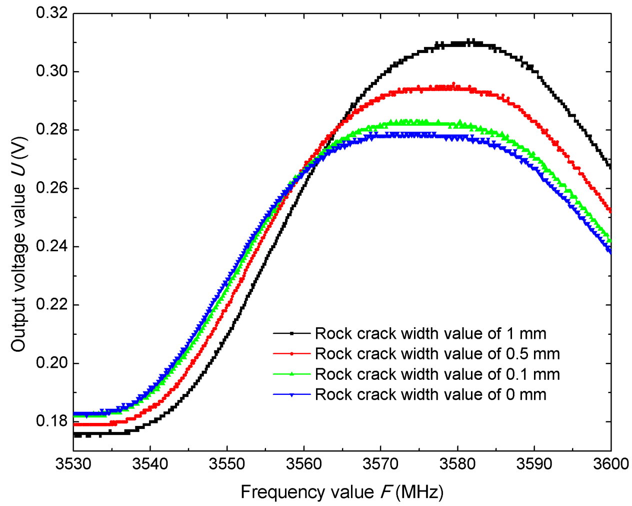

FIGURE 8. Relationship curve between output voltage value *U* (V) and resonance vibration frequency *F* (MHz) in granite specimen.

are measured under the condition that the plug gauge is a standard and the results are shown in Fig. 7. Three or more tests were repeated for each case with the same rock crack width to minimize the dispersion of test results. Next, under the same test conditions, the rock crack widths of 0 to 1 mm are measured under the condition that the dial gauge is a standard, and the results are shown in Fig. 7. Correspondingly, three or more tests were repeated for each case with the same rock crack width to minimize the dispersion of test results. Subsequently, the experimental calibration taking dial gauge as a standard was determined for the later experiment after the above comparison. Fig. 7 shows a comparison of the two experimental calibration methods. These measurement results in Fig. 7 are discussed in subsection III.A below. Second, the effects of installation conditions and humidity conditions on rock crack width measurement were studied, and the relative error of the system was analyzed. A minimum recognition ability experiment for a crack width of 5 μm was made.

III. RESULTS AND DISCUSSION

A. COMPARISON OF MEASUREMENT ACCURACY BETWEEN THE PLUG GAUGE AND DIAL GAUGE

In this section, the measurement results of rock crack width are evaluated by comparing the differences in rock crack width measurement accuracy, which is calibrated by taking the plug gauge or the dial gauge as a standard. The experimental ambient temperature was 29 °C and the relative humidity was 44.8 %. First, in Fig. 8, it shows the relationship curve between the output voltage value *U* (V) of measuring apparatus and resonance vibration frequency value *F* (MHz) in regular crack widths measurement of granite specimen. It should be noted that, in order to observe that the sensor output voltage increases as the rock crack width increases, the curve is set to be convex as opposed to Fig. 3. To facilitate brevity, only four test points are listed, and the corresponding crack width measurement values are 0, 0.1, 0.5, and 1 mm, respectively. The other data is given in Fig. 7 and is analyzed as follows. As seen from Fig. 8, it is feasible to measure the rock crack width based on the microwave resonance vibration model. Next, compare the differences in rock crack widths measurement accuracy using the calibration taking the plug gauge or the dial gauge as a standard, as shown in Fig. 7. Fig. 7 is a graph showing the relationship between the rock crack width actual measurement value *M* (mm) of measuring apparatus and the crack width value *G* (mm) of granite under the condition of taking the plug gauge or the dial gauge as a standard. Each test point corresponds to an average value whose value is the average of three repeated measurements of the same rock crack width. As seen from Fig. 7, the linearity of the measurement results by taking the dial gauge calibration is obviously more superior. By comparison, the human operation error of the plug gauge is more apparent. Even so, the experimental results still show that the rock crack width measuring system based on microwave resonance vibration model shows good linearity. To improve accuracy, the experiment times of each rock crack width measuring could be increased. Such measures will be described in section III.C.

B. INFLUENCE OF ENVIRONMENTAL CONDITIONS ON EXPERIMENTAL RESULTS

The experiment of rock crack width determination was carried out indoor with controlled temperature and environmental relative humidity to simulate the influence of outdoor environmental conditions on the experimental measurement results. Here, data analysis is performed by taking one measurement result of the regular crack widths in a granite specimen as an example. Fig. 9 is a graph showing the relationship between the output voltage value *U* (V) of measuring apparatus and the crack width value *G* (mm) under various

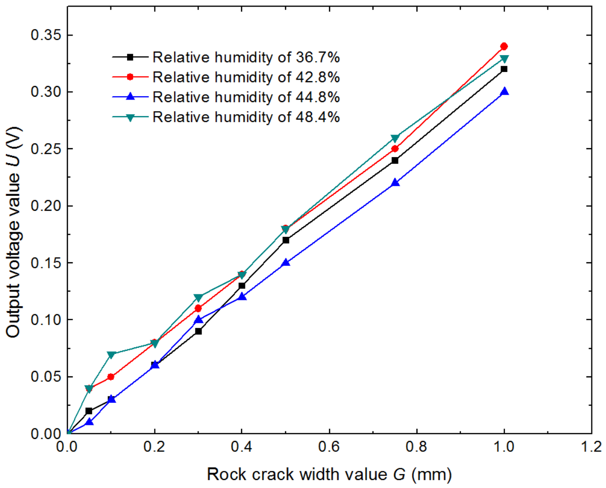

FIGURE 9. Influence of relative humidity on granite crack width measurement.

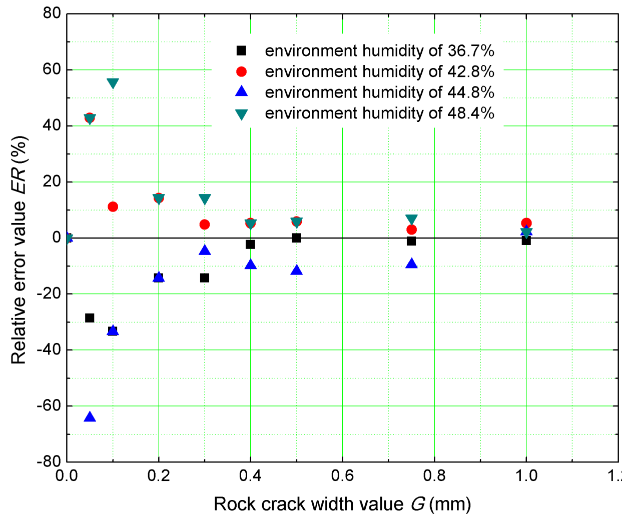

FIGURE 10. Relative error curve of granite crack width measurement.

environmental conditions, which corresponds the relative humidity of 36.7%, 42.8%, 44.8%, and 48.4%. It can be seen from Fig. 9 that the four curves do not completely coincide, indicating that changes in ambient temperature and relative humidity have an effect on the measurement results, where the change is small. In addition, the above results also show that changes in ambient temperature and relative humidity do not affect the linearity of the system. The experimental results further prove the good linearity of the rock crack width measuring system based on microwave resonance vibration model. The environmental relative humidity range studied in this section is still relatively small. The effects of wider environmental relative humidity conditions on irregular crack specimens will be discussed in Section III.E. When considering the influence of the extreme saturated state on the experimental results, for example, after the test specimen is soaked in water, the influence of the increase of the specimen water content on the measurement result is still large. The results of these experiments are discussed in Section III.E below.

C. ANALYSIS OF RELATIVE ERROR

This section will make a relative error analysis of regular crack width measurements of granite specimen under various temperature and relative humidity conditions. One of the measurement results is taken as a case of the data analysis. The values of U_1, U_2, U_3 and U_4 corresponding to rock crack width value G (mm) are substituted into "(11)" to obtain the average value. Here, the value of U_1, U_2, U_3 and U_4 respectively represent the output voltage value corresponding to the relative humidity of 36.7%, 42.8%, 44.8%, and 48.4%. Then, the difference is calculated and the relative error found, as shown in Fig. 10. Fig. 10 is a graph showing the relationship between the relative error value ER (%) of measuring apparatus and the crack width value G (mm) of granite. It can be seen from Fig. 10 that the relative error at G (mm) $= 0.05$ (mm) is significantly larger, and the maximum relative error value reaches -64%. The maximum error at G (mm) $= 1$ (mm) is 5%. From the perspective of the minimum rock crack width and the maximum rock crack width, the relative error mainly occurs at the portion of the small one. After analyzing the measurement results, it is believed that the relative error of rock crack width measurement based on microwave resonance vibration model is mainly derived from two aspects, which means the measurement system is affected by electromagnetic noise interference and humidity. There are examples of analyzing the type of interference. For instance, with ambient temperature 21 °C and relative humidity 79%, when the test system input U_i is 0V, the system output U_{omax} is not 0 V but 1.298 V is recorded with an oscilloscope. In another case, when the system input signal amplitude U_i is 0.223 V and the frequency f_0 is 3.7 GHz, the oscilloscope records the system output U_{omax} is 2.542 V, while the normal value U_{omax} should be 1.320 V. These situations indicate that the system has suffered severe interference. After scaling, it will be followed by a gross error. In order to solve such interference problems, high-pass filtering measures have been added to the hardware. Data processing adopts multiple digital filtering measures, such as probability statistics method to remove gross errors caused by random interference in the same frequency band, and the mean filtering model (Eq. "(11)") to eliminate gross errors caused by non-periodic random interference signals of background noise. In addition, the iron metal shield cover is adopted to isolate the circuit board from the outside space, eliminating external electromagnetic interference. After adding the above measures, the relative error is greatly reduced, and the results are shown in Fig. 11(a)(b). Fig. 11(a) is a graph showing the relationship between the output voltage values U (V) or the relative error value ER (%) of measuring apparatus and the crack width value G (mm) of granite. Fig. 11(b) is a graph showing the relationship between the rock crack width actual measurement values M (mm) or the relative error value ER (%) of measuring

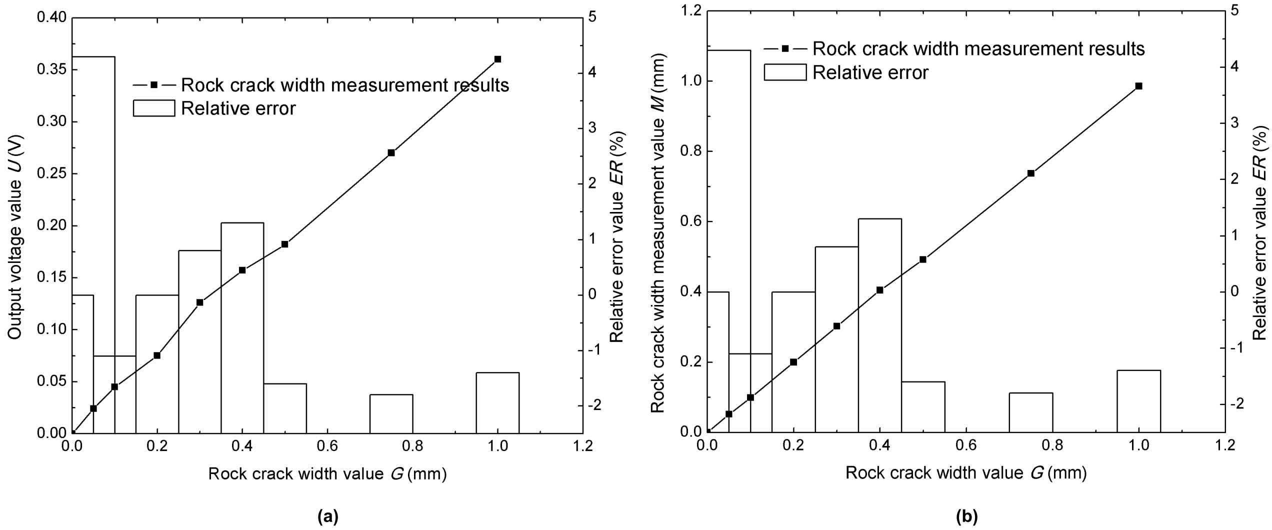

FIGURE 11. Crack width measurement curve or relative error curve of granite under the condition of 100 repeated experiments.

apparatus and the crack width value G (mm) of granite. The results show that the maximum error does not exceed $\pm 5\%$, which proves that the rock crack width measuring system based on microwave resonance vibration model has good repeatability and stability.

$$\bar{U} = \frac{1}{n}(\sum_{i=1}^{n} Ui) \tag{11}$$

where $\bar{U}$ is the average of output voltage, and U_i is the output voltage, $n = 2, 3, 4,$.

D. DISCUSSION OF MINIMUM RECOGNITION ABILITY

Based on the above discussion of the factors affecting the accuracy of rock crack width measurement, the minimum recognition ability of crack width measurement method is mainly discussed here. Fig. 12 shows the experimental results of the minimum recognition ability in the granite crack width measurement with a regular crack. Fig. 12 shows a graph of the relationship between the output voltage value U (V) of measuring apparatus and the resonance vibration frequency value F (MHz). The experimental ambient temperature was 29 °C and the relative humidity was 44.8%. The results show that the method of measuring rock crack widths based on microwave resonance vibration model can capture a crack width of 5μm, and the above experimental results were obtained with a resonance vibration frequency of 3.575 GHz. In other words, when the smallest crack width is 5 μm, the sensor begins to react. While the minimum value of the system stability detection is 50 μm. The response speed of the sensor is closely related to the resonance oscillation frequency. The response speed of the sensor increases as the number of changes in the resonance oscillation period increases. When the rock specimen and sensor are coupled, the resonance oscillation frequency will be disturbed. From the moment of disturbance, to the time required for final stabilization, it takes at least one cycle time. Therefore, the response speed of the sensor is as fast as approximately 0.28 ns. After the analysis of the minimum recognition ability of measuring rock crack width based on microwave resonance vibration model, it would be interesting to investigate how well this method could capture the cracks initiation in rock specimen. As this study focuses on the detection of micro small rock crack widths, the maximum rock crack width given in the above section is only 1 mm. It is noted that the measurable rock crack width is higher than 1 mm.

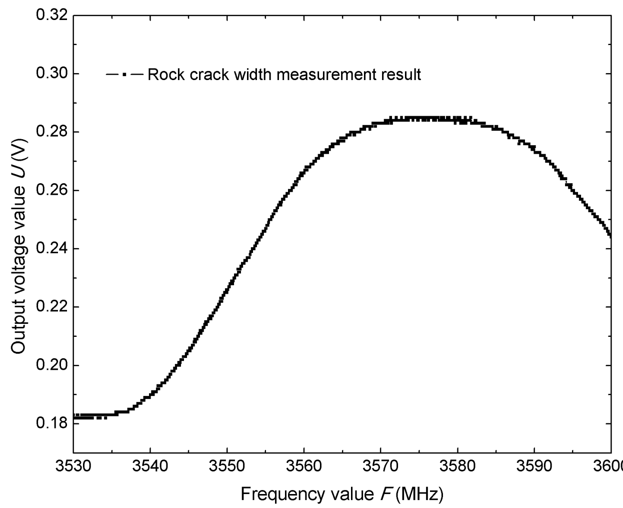

FIGURE 12. Relationship curve between output voltage value *U* (V) and resonance vibration frequency *F* (MHz) in granite specimen.

E. MEASUREMENT OF IRREGULAR ROCK CRACK WIDTH AND ANALYSIS OF INFLUENCING FACTORS

This section attempts to measure the irregular crack width of rock and discuss the influence of the specimen installation conditions (including the specimen surface roughness

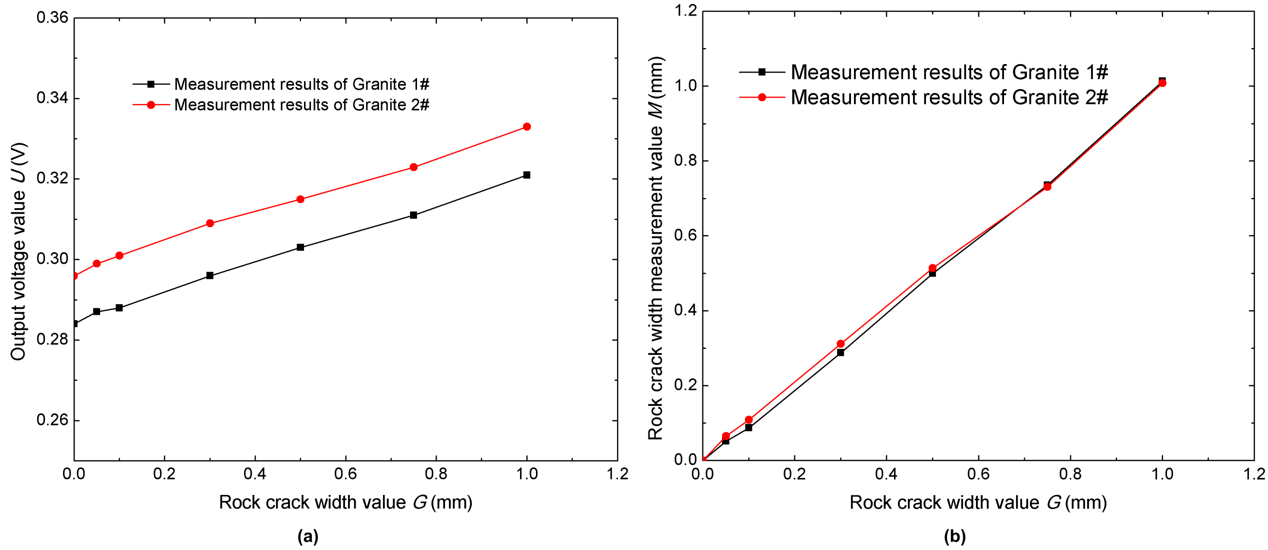

FIGURE 13. Measurement results of irregular rock crack width.

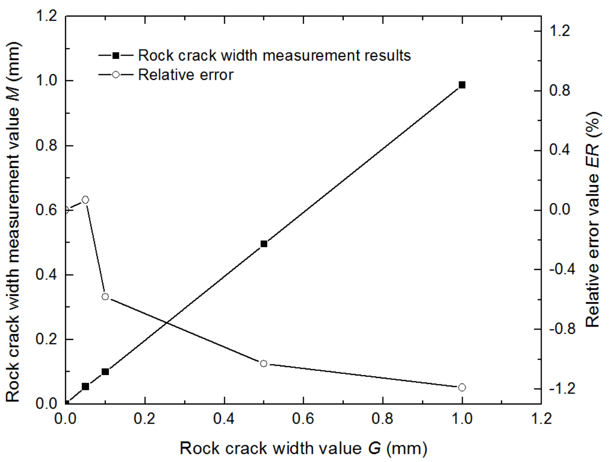

FIGURE 14. Influence of regular crack specimen surface roughness R_a on measurement results (D is 0.1mm).

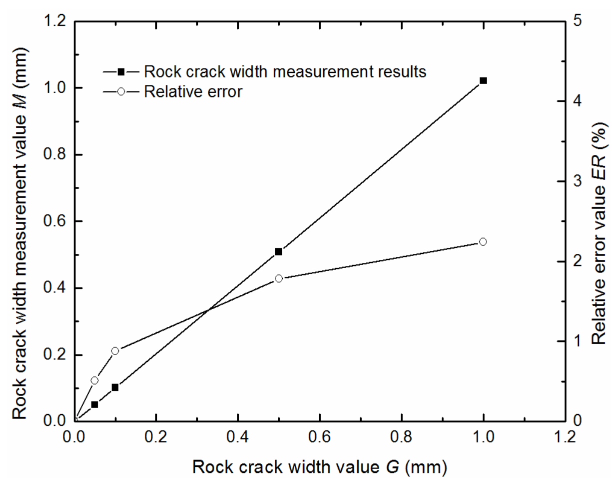

FIGURE 15. The effect of D from 0.1mm to 0.194mm on the measured results of 1# irregular crack specimen.

R_a and the standoff distance D) and humidity conditions (the wider range environmental relative humidity conditions and the specimen water content) on the measurement results. After calibrating according to the foregoing method, two granite specimens with irregular crack were experimentally studied in order to observe whether the regular crack width measurement method in rock can be applied to the irregular crack width detection. The measurement results are displayed in Fig. 13. Fig. 13(a) is a graph showing the relationship between the output voltage value U (V) of measuring apparatus and the crack width value G (mm) of granite 1# or 2#. Fig. 13(b) is a graph showing the relationship between the rock crack width actual measurement value M (mm) of measuring apparatus and the crack width value G (mm) of granite 1# or 2#. As seen from Fig. 13(a), the voltage output value of granite 2# is larger than the voltage output value of granite 1#, but as seen from Fig. 13(b), the linearity of the two curves is good. From the above, it can be concluded that the measuring approach based on microwave resonance vibration model of the regular crack width in rock can be directly applied to the irregular one.

The effect of the specimen surface roughness R_a is discussed below. When the standoff distance D is 0.1 mm, the influence of the surface roughness R_a of the regular crack specimen on the measurement result is shown in Fig. 14. It shows the relationship between the rock crack width actual measurement values M (mm) or the relative error value ER (%) of measuring apparatus and the crack width value G (mm) of regular crack specimen. The surface roughness Ra, that is, pre-fabricated pits of different diameters (i.e. 20μm~300μm) on the specimen surface. The variation of the surface roughness R_a of the regular crack specimen

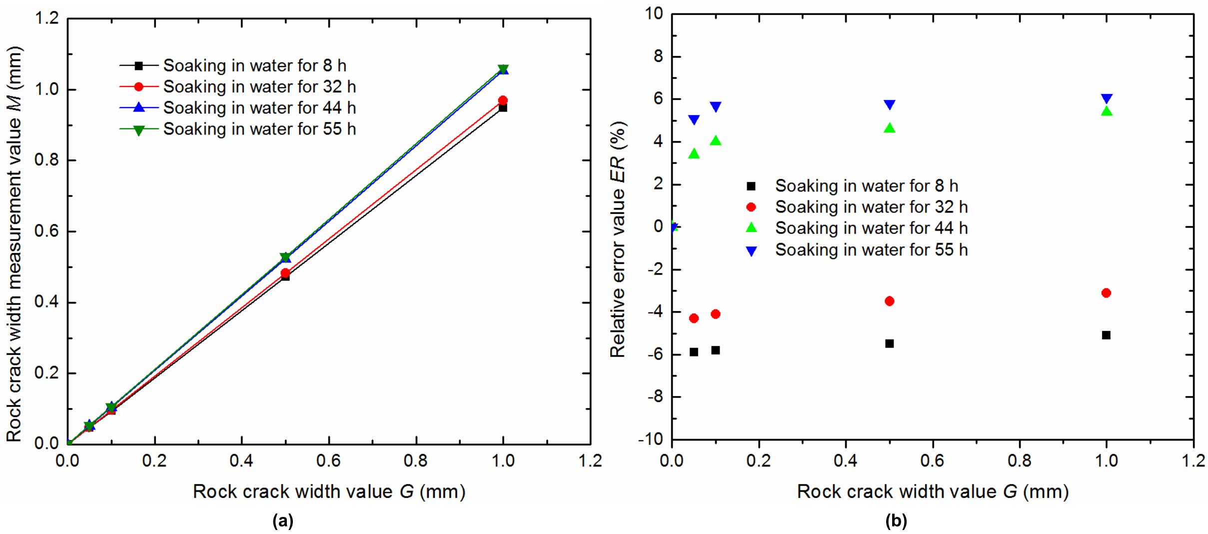

FIGURE 16. Influence of different water content of 1# irregular crack specimen on measurement results.

only affects the measurement accuracy, and the resonance oscillation frequency point will not change. As shown in the Fig. 14, the maximum measurement error is -1.19 %.

In the following step, when loading the specimen, the influence of the standoff distance D should be payed attention. For example, when the standoff distance D changes from 0.1 mm to 0.194 mm, the peak resonance vibration frequency of irregular crack changes from 3.544 GHz to 3.546 GHz, which is deviated from 2.0 MHz. And the system measurement error is shown in Fig. 15. It indicates the relationship between the rock crack width actual measurement values M (mm) or the relative error value ER (%) of measuring apparatus and the crack width value G (mm) of 1# irregular crack specimen. As can be seen from the Fig. 15, the maximum measurement error is 2.24 %.

Afterwards, a wider range of environmental relative humidity impact experiments were supplemented to examine the performance of the device. At ambient temperature of 27°, four kinds of relative humidity effects on experiments such as 30%, 48.4%, 70%, 90 % were carried out on the 1# irregular crack specimen. And the measurement results were compared with the measurement results of 48.4 %*RH* of the above regular crack specimen, and the results are shown in Table 1. The symbol "MRs" indicates the measurement results. It can be seen that different relative humidity influence the measurement results, and 90 %*RH* has the greatest influence on the measurement results, which is 3.3% larger than the measurement error of regular crack in the case of 48.4 %*RH*.

It is also important that the water content of rock could affect the accuracy of rock crack width measurements. As shown in Fig. 16, the experimental results are obtained after the test specimen soaked for 8, 32, 44, 55 hours. Fig. 16 shows the influence of different water content of 1# irregular crack specimen on measurement results. The water content of the test specimen obtained by soaking the specimen for 8, 32, 44, and 55 hours were 0.155%, 0.201%, 0.232%, and 0.263 %, respectively. It can be found that if the test specimen is soaking in water for different hours, which means the water content is different. The measurement errors are different, and the maximum error is 6.1 % accordingly. It should be pointed out, the water absorption of rock specimens changes less and less with the prolongation of rock soaking time. Therefore, for the test specimen soaking in water for 44h, a layer of water film is attached to the specimen surface and the experiment was carried out afterwards. While for the test specimen soaked in water for 55h, a thicker water film is attached to the specimen surface. That is, the test specimen with the greatest water content and the test specimen with a thick water film on surface has the largest measurement error.

TABLE 1. Measurement errors of 1# irregular crack specimen under different relative humidity conditions.

Rock crack width value	MRs of 30 %*RH*	MRs of 48.4 %*RH*	MRs of 70 %*RH*	MRs of 90 %*RH*
G (mm)	*ER* (%)	*ER* (%)	*ER* (%)	*ER* (%)
0.05	0.1	0	1.5	3.3
0.1	-1.3	0	1.8	1
0.5	0	0	0	0
1	0	0	0.8	1.6

IV. CONCLUSION

To accurately determine micro crack widths using a simple and cost-effective test technique, a new approach based on the microwave resonance vibration model for rock material crack width detection was proposed in the present paper.

Experimental verification of microwave resonance vibration model-based measurement method with a central frequency of 3.665 GHz was carried out on the crack width of 0 to 1mm of granite material. Experimental calibration was carried out by taking the plug gauge and the dial gauge as standard. The experiments include the determination of the regular straight crack width in rock and the irregular one. Simultaneously, the influence of environmental relative humidity and specimen water content on measurement results is discussed, and the relative error of the experimental results and the minimum recognition ability of the detection system are discussed. And the findings of the study are summarized as follows:

(1) It is possible to successfully measure the prefabricated rock crack width by a microwave resonance vibration model-based measurement method with a central frequency of several GHz, a method which is especially suitable for micro crack detection. When the rock crack width is set to 5 μm, the device can detect it, but the instability error is large. In fact, the minimum stable detection of the system is 50 μm. And the measurable rock crack width is greater than 1 mm.

(2) The method of measuring rock crack width based on the microwave resonance vibration model proposed in the present paper has a fast response speed, and its response speed reaches 0.28 ns.

(3) In this paper, the random interference of the measurement system is discussed. After filtering measures are taken, the measurement error is significantly reduced, and the relative error of the measurement system reaches ± 5 %. From the experimental results, the linearity of the detection systems is good.

(4) Influencing factors such as sample installation conditions, environmental relative humidity and specimen water content were discussed. The experimental results show that these have certain effects on rock crack width measurement results.

Therefore, the new method for determining rock crack width is suitable for monitoring micro cracks in rocks and can help in the monitoring of rocks width deformations, as well as in rock engineering stability evaluation. Owing to the fast response of the method proposed in the present paper, the capture of crack initiation in rock materials is achievable and needs to be tested in the next step. In addition, the next step is to perform deep positioning and algorithm-based visualizing for the hidden cracks in rocks.

APPENDIX

$\boldsymbol{E}$ electric field strength vector
$E0$ electric field strength amplitude value, which is a constant
γ propagation constant in space
x propagation distance along the x-axis
$j\omega$ resonance vibration angular frequency
t time required for one oscillation cycle
α decay constant
$j\beta$ phase constant
σ conductivity
ε dielectric constant
μ magnetic permeability
$\boldsymbol{Z}$ wave impedance
$\boldsymbol{H}$ magnetic field strength vector
d microwave penetration depth
Γ reflection coefficient
Z_1 air dielectric wave impedance
Z_2 wave impedance in rock specimen
ω_0 resonance oscillation angular frequency
L_0 sum of the equivalent of sensor inductance and distribution parameter
C_0 sum of the equivalent of the distribution parameters of sensor and resonance oscillation circuit capacitance
f_0 resonance oscillation frequency
U_0 resonance vibration output voltage
U_S equivalent output voltage of microwave resonance oscillation signal
U_R equivalent total resistance voltage
$\bar{U}$ average of output voltage, and
U_i output voltage, n = 2, 3, 4,

REFERENCES

[1] G. Su et al., "True triaxial experimental study of rockbursts induced by ramp and cyclic dynamic disturbances," Rock Mech. Rock Eng., vol. 51, no. 4, pp. 1027–1045, 2017. doi: 10.1007/s00603-017-1384-y.
[2] W. Gong, Y. Peng, H. Wang, M. He, L. R. Sousa, and J. Wang, "Fracture angle analysis of rock burst faulting planes based on true-triaxial experiment," Rock Mech. Rock Eng., vol. 48, no. 3, pp. 1017–1039, 2015. doi: 10.1007/s00603-014-0639-0.
[3] J. Teng, J. Tang, Y. Zhang, and X. Li, "CT experimental study on the damage characteristics of anchored layered rocks," KSCE J. Civil Eng., vol. 22, no. 9, pp. 3653–3662, 2018. doi: 10.1007/s12205-018-0425-8.
[4] Y. Wang, C. H. Li, and Y. Z. Hu, "X-ray computed tomography (CT) observations of crack damage evolution in soil-rock mixture during uniaxial deformation," Arabian J. Geosci., vol. 11, no. 9, p. 199, May 2018. doi: 10.1007/s12517-018-3561-z.
[5] M. D. Ingraham, K. A. Issen, and D. J. Holcomb, "Use of acoustic emissions to investigate localization in high-porosity sandstone subjected to true triaxial stresses," Acta Geotechn., vol. 8, no. 6, pp. 645–663, 2013. doi: 10.1007/s11440-013-0275-y.
[6] X. G. Zhao et al., "Influence of unloading rate on the strainburst characteristics of Beishan granite under true-triaxial unloading conditions," Rock Mech. Rock Eng., vol. 47, no. 2, pp. 467–483, 2014. doi: 10.1007/s00603-013-0443-2.
[7] Y. Farnam, M. R. Geiker, D. Bentz, and J. Weiss, "Acoustic emission waveform characterization of crack origin and mode in fractured and ASR damaged concrete," Cement Concrete Compos., vol. 60, pp. 135–145, Jul. 2015. doi: 10.1016/j.cemconcomp.2015.04.008.
[8] A. Carpinteri, G. Lacidogna, A. Manuello, G. Niccolini, A. Schiavi, and A. Agosto, "Mechanical and electromagnetic emissions related to stress-induced cracks," Experim. Techn., vol. 36, no. 3, pp. 53–64, 2012. doi: 10.1111/j.1747-1567.2011.00709.x.
[9] J.-L. Li, K.-P. Zhou, W.-J. Liu, and H.-W. Deng, "NMR research on deterioration characteristics of microscopic structure of sandstones in freeze–thaw cycles," Trans. Nonferrous Metals Soc. China, vol. 26, no. 11, pp. 2997–3003, 2016. doi: 10.1016/S1003-6326(16)64430-8.
[10] J. Li, R. B. Kaunda, and K. Zhou, "Experimental investigations on the effects of ambient freeze-thaw cycling on dynamic properties and rock pore structure deterioration of sandstone," Cold Regions Sci. Technol., vol. 154, pp. 133–141, Oct. 2018. doi: 10.1016/j.coldregions.2018.06.015.

[11] K. Zhou, T. Liu, and Z. Hu, "Exploration of damage evolution in marble due to lateral unloading using nuclear magnetic resonance," *Eng. Geol.*, vol. 244, pp. 75–85, Oct. 2018. doi: 10.1016/j.enggeo.2018.08.001.
[12] Y. Zhang, S. Jin, Y. Wang, and Y. Wang, "Characterization of the pore size distribution with SEM images processing for the tight rock," in *Proc. IEEE Int. Conf. Inf. Automat.*, Aug. 2015, pp. 653–656. doi: 10.1109/ICInfA.2015.7279367.
[13] Z. He, G. Li, S. Tian, H. Wang, Z. Shen, and J. Li, "SEM analysis on rock failure mechanism by supercritical CO_2 jet impingement," *J. Petroleum Sci. Eng.*, vol. 146, pp. 111–120, Oct. 2016. doi: 10.1016/j.petrol.2016.04.023.
[14] B. M. Abdullah, J. Cullen, A. Mason, and A. I. Al-Shamma'a, "A novel method for monitoring structural metallic materials using microwave NDT," in *Sensing Technology: Current Status and Future Trends*, vol. 7, A. Mason, S. C. Mukhopadhyay, K. Jayasundera, and N. Bhattacharyya, Eds. Cham, Switzerland: Springer, 2014, pp. 161–180. doi: 10.1007/978-3-319-02318-2_9.
[15] S. Kharkovsky, A. McClanahan, R. Zoughi, and D. D. Palmer, "Microwave dielectric-loaded rectangular waveguide resonator for depth evaluation of shallow flaws in metals," *IEEE Trans. Instrum. Meas.*, vol. 60, no. 12, pp. 3923–3930, Dec. 2011. doi: 10.1109/TIM.2011.2149370.
[16] M. S. ur Rahman, A. Yassin, and M. A. Abou-Khousa, "Microwave imaging of thick composite structures using circular aperture probe," *Meas. Sci. Technol.*, vol. 29, no. 9, Sep. 2018, Art. no. 095403. doi: 10.1088/1361-6501/aad2cf.
[17] Y. Ju, M. Saka, and Y. Uchimura, "Evaluation of the shape and size of 3D cracks using microwaves," *NDT&E Int.*, vol. 38, no. 8, pp. 726–731, Dec. 2005. doi: 10.1016/j.ndteint.2005.02.009.
[18] U. Nitsan, "Electromagnetic emission accompanying fracture of quartz-bearing rocks," *Geophys. Res. Lett.*, vol. 4, no. 8, pp. 333–336, Aug. 1977. doi: 10.1029/GL004i008p00333.
[19] B. T. Brady and G. A. Rowell, "Laboratory investigation of the electrodynamics of rock fracture," *Nature*, vol. 321, no. 29, pp. 488–492, 1986. doi: 10.1038/321488a0.
[20] T. Ogawa, K. Oike, and T. Miura, "Electromagnetic radiations from rocks," *J. Geophys. Res.*, vol. 90, no. D4, pp. 6245–6249, Jun. 1985. doi: 10.1029/jd090id04p06245.
[21] I. Yamada, K. Masuda, and H. Mizutani, "Electromagnetic and acoustic emission associated with rock fracture," *Phys. Earth Planet. Interiors*, vol. 57, pp. 157–168, Oct. 1989. doi: 10.1016/0031-9201(89)90225-2.
[22] A. Tsutsumi, S. Tanaka, N. Shirai, and Y. Enomoto, "Electric signals accompanying fracture of granite," *Jpn. J. Appl. Phys.*, vol. 42, pp. 5208–5212, Aug. 2003. doi: 10.1143/JJAP.42.5208.
[23] C. Mavromatou, V. Hadjicontis, D. Ninos, D. Mastrogiannis, E. Hadjicontis, and K. Eftaxias, "Understanding the fracture phenomena in inhomogeneous rock samples and ionic crystals, by monitoring the electromagnetic emission during their deformation," *Phys. Chem. Earth A/B/C*, vol. 29, nos. 4–9, pp. 353–357, 2004. doi: 10.1016/j.pce.2003.11.011.
[24] D. Song, E. Wang, and J. Liu, "Relationship between EMR and dissipated energy of coal rock mass during cyclic loading process," *Saf. Sci.*, vol. 50, no. 4, pp. 751–760, Apr. 2012. doi: 10.1016/j.ssci.2011.08.039.
[25] D. Song, E. Wang, X. Song, P. Jin, and L. Qiu, "Changes in frequency of electromagnetic radiation from loaded coal rock," *Rock Mech. Rock Eng.*, vol. 49, no. 1, pp. 291–302, Jan. 2016. doi: 10.1007/s00603-015-0738-6.
[26] T. Zhu, J. Zhou, and H. Wang, "Electromagnetic emissions during dilating fracture of a rock," *J. Asian Earth Sci.*, vol. 73, no. 8, pp. 252–262, Sep. 2013. doi: 10.1016/j.jseaes.2013.05.004.
[27] S. O. Gade, B. B. Alaca, and M. G. R. Sause, "Determination of crack surface orientation in carbon fibre reinforced polymers by measuring electromagnetic emission," *J. Nondestruct. Eval.*, vol. 36, no. 2, p. 21, 2017. doi: 10.1007/s10921-017-0403-y.
[28] S. O. Gade and M. G. R. Sause, "Measurement and study of electromagnetic emission generated by tensile fracture of polymers and carbon fibres," *J. Nondestruct. Eval.*, vol. 36, p. 9, Mar. 2017. doi: 10.1007/s10921-016-0386-0.
[29] S. O. Gade, U. Weiss, M. A. Peter, and M. G. R. Sause, "Relation of electromagnetic emission and crack dynamics in epoxy resin materials," *J. Nondestruct. Eval.*, vol. 33, no. 4, pp. 711–723, Dec. 2014. doi: 10.1007/s10921-014-0265-5.
[30] S. Hu, E. Wang, Z. Li, R. Shen, and J. Liu, "Time-varying multifractal characteristics and formation mechanism of loaded coal electromagnetic radiation," *Rock Mech. Rock Eng.*, vol. 47, no. 5, pp. 1821–1838, 2014. doi: 10.1007/s00603-013-0501-9.
[31] M. Nicco, E. A. Holley, P. Hartlieb, R. Kaunda, and P. P. Nelson, "Methods for characterizing cracks induced in rock," *Rock Mech. Rock Eng.*, vol. 51, no. 7, pp. 2075–2093, Jul. 2018. doi: 10.1007/s00603-018-1445-x.
[32] A. Perino, R. Orta, and G. Barla, "Wave propagation in discontinuous media by the scattering matrix method," *Rock Mech. Rock Eng.*, vol. 45, no. 5, pp. 901–918, 2012. doi: 10.1007/s00603-012-0286-2.
[33] B. Wang, Z. Guo, Y. Han, and T. Zhang, "Electromagnetic wave absorbing properties of multi-walled carbon nanotube/cement composites," *Construct. Building Mater.*, vol. 46, pp. 98–103, Sep. 2013. doi: 10.1016/j.conbuildmat.2013.04.006.
[34] X. Lv, Y. Duan, and G. Chen, "Electromagnetic wave absorption properties of cement-based composites filled with graphene nano-platelets and hollow glass microspheres," *Construct. Building Mater.*, vol. 162, pp. 280–285, Feb. 2018. doi: 10.1016/j.conbuildmat.2017.12.047.
[35] C. Liao, *Foundation of Microwave Technology*. Xi'an, China: Xidian Univ. Press, 2004, pp. 16–44.

CHUANJING OU received the B.S. degree in civil engineering, and the M.S. degrees in geotechnical engineering from the Guilin University of Technology, China, in 2012 and 2015, respectively. She is currently pursuing the Ph.D. degree in geotechnical engineering with Central South University, China. Her research interests include civil engineering, geotechnical engineering, and rock mechanics.

PING CAO received the Ph.D. degree in rock mechanics from Central South University, China, in 1990, where he is currently a Professor and the Doctoral Supervisor with the School of Resources and Safety Engineering. He is the Director of the Center for Mineral Rock Engineering Mechanics, Central South University. His research interests include the theory and application of rock mechanics. He is a member of the Chinese Society for Rock Mechanics and Engineering, and a member of the International Society of Rock Mechanics.

YU CHEN received the Ph.D. degree in engineering geology and rock mechanics from the Norwegian University of Science and Technology, Norway, in 2015. He is currently an Associate Professor with the School of Resources and Safety Engineering, Central South University. His research interests include rock mechanics and anchor-pile support.

JINFENG HE was born in Guangxi Zhuang Autonomous Region, China, in 1969.

He is the Director of the Guangxi Electronic Products Quality Inspection Center, Beihai, China. He is a Senior Engineer and a registered national jewelry jade quality inspector. He has been engaged in jewelry appraisal, grading evaluation, and electronic product quality inspection and management. He presided over or participated in five provincial and ministerial projects. He has participated in the formulation of two national standards and five local standards. So far, he has published eight papers, obtained five invention patents, and three computer software copyrights.

XIANWEN LIAO received the B.S. degree in information and computing science, and the M.S. degree in software engineering from the Xi'an University of Science and Technology, China, in 2004 and 2017, respectively. He is currently pursuing the Ph.D. degree in communication engineering with the Guilin University of Electronic Technology.

From 2004 to 2011, he was a Software Engineer and the Project Manager, and has been involved in software research and development of powerful automation and communication in the software enterprise. During this time, he also worked on neural networks and optimization. He came to the Guilin University of Electronic Technology to teach software engineering course, in 2011, and obtained the certification of Information System Project Manager, in 2015. His current research interests are data mining and natural language processing. He has published four papers and received a patent for utility models.

HONGCAI CHEN received the B.S. degree in electronic information engineering from the Guilin University of Electronic Technology, China, in 2012. He is currently an Engineer with the Guangxi Electronic Products Quality Inspection Center. In the past three years, he has published three papers, and has participated in the standard formulation and patent project. He has been awarded the advanced individual of 2014, 2016, and 2017, respectively. His research interests include the development of experimental devices and the application of rock mechanics. He is a member of the pool of experts under the supervision of the state.

JINGJING MENG received the Ph.D. degree in civil engineering from The University of Newcastle, Australia, in 2017. His research interests include numerical modelling and rock mechanics. He is currently developing an innovative discrete element method based on the interior-point method which is more efficient when modeling static problems and high stiffness materials. The method is used and validated through modeling granular materials and rock fracture problems.